

Possible signatures of mixed-parity superconductivity in doped polar SrTiO₃ filmsTimo Schumann,^{*} Luca Galletti[✉],^{*} Hanbyeol Jeong[✉], Kaveh Ahadi, William M. Strickland[✉],
Salva Salmani-Rezaie, and Susanne Stemmer[†]*Materials Department, University of California, Santa Barbara, California 93106-5050, USA*

(Received 5 December 2019; accepted 9 March 2020; published 23 March 2020)

Superconductors that possess both broken spatial inversion symmetry and spin-orbit interactions exhibit a mix of spin singlet and triplet pairing. Here, we report on measurements of the superconducting properties of electron-doped, strained SrTiO₃ films. These films have an enhanced superconducting transition temperature and were previously shown to undergo a transition to a polar phase prior to becoming superconducting. We show that some films show signatures of an unusual superconducting state, such as an in-plane critical field that is higher than both the paramagnetic and orbital pair breaking limits. Moreover, nonreciprocal transport, which reflects the ratio of odd versus even pairing interactions, is observed. Together, these characteristics indicate that these films provide a tunable platform for investigations of unconventional superconductivity.

DOI: [10.1103/PhysRevB.101.100503](https://doi.org/10.1103/PhysRevB.101.100503)

Topological superconductors can host quasiparticle states that offer a promising route for generating quantum entangled states that are protected against decoherence [1]. While many of the approaches that are currently being pursued involve hybrid structures [2–5], the discovery of an *intrinsic* topological superconductor would be an exciting step forward. One route involves finding superconductors that possess both broken spatial inversion symmetry and spin-orbit interactions, which are expected to exhibit a mix of singlet and triplet pairing due to the lifting of the twofold spin degeneracy [6–9]. The application of a Zeeman field or other microscopic interactions can suppress the *s*-wave channel in favor of odd-parity superconductivity [8].

Bulk, unstrained SrTiO₃ is a multiband superconductor [10–12] that exhibits a superconducting dome with a maximum transition temperature (T_C) of ~ 300 mK at a carrier density of $1 \times 10^{20} \text{ cm}^{-3}$ [13]. The degeneracy of the three t_{2g} -derived conduction bands at the Γ point is lifted by the low-temperature tetragonal distortion and by spin-orbit coupling [14,15]. With increasing carrier density, the three bands fill consecutively [15–17]. Quasi-two-dimensional electron systems at interfaces involving SrTiO₃, which exhibit signatures of Rashba spin-orbit coupling [18–22], have been suggested as possible candidates for topological superconductivity [8,23]. Bulk SrTiO₃ is also a quantum paraelectric [24] that is near a ferroelectric transition. The fixed polarization charge of ferroelectrics, and corresponding electric fields, can easily rival those of high-density two-dimensional electron gases [25]. Early theoretical work already pointed out that ferroelectric order would be a promising route to realize odd-parity superconductivity [6]. Combining the ingredients of multiorbital effects, ferroelectricity, and spin-orbit coupling, a topological superconducting state has been predicted [26,27].

Recently, it was shown that ferroelectric (polar), doped SrTiO₃ can become superconducting [28–32]. In particular, doped SrTiO₃ films grown on (001) (LaAlO₃)_{0.3}(Sr₂AlTaO₆)_{0.7} (LSAT), which are compressively strained, undergo a transition to a ferroelectric phase prior to becoming superconducting and show enhanced superconducting transition temperatures [28,29]. Because of the broken inversion symmetry, such films are promising candidates in the search for an intrinsic topological superconductor.

A key signature of odd- or mixed-parity superconductors is an enhancement of the upper critical field beyond the paramagnetic (Clogston-Chandrasekhar or Pauli) limit [8]. Here, we show that some polar superconducting SrTiO₃ films show anisotropic critical fields above the Pauli limit. Moreover, we find pronounced nonreciprocal charge transport, a signature of a noncentrosymmetric, spin-orbit coupled superconductor that is sensitive to the parity of the superconducting order parameter [33,34]. Taken together, these observations indicate a highly unconventional superconductor.

Doped SrTiO₃ films were grown by hybrid metal-organic molecular beam epitaxy [35,36]. Strained films with thicknesses between 160 and 180 nm were grown on (001) (LaAlO₃)_{0.3}(Sr₂AlTaO₆)_{0.7} (LSAT) crystals. The lattice mismatch between SrTiO₃ ($a = 3.905 \text{ \AA}$) and LSAT ($a = 3.868 \text{ \AA}$) is -0.95% . Some of the films were coherently strained (such as film A discussed below), while others (such as the films denoted B and D in the following) were partially relaxed. Details of the films' structure can be found in the Supplemental Material [37]. All films were *n*-type doped by substituting Sr²⁺ with either La³⁺ or Sm³⁺. The choice of dopant had no influence on the superconducting parameters, such as critical field (H_{c2}) and critical temperature (T_C). Electrical measurements were performed on Hall bar devices with dimensions of $100 \mu\text{m} \times 100 \mu\text{m}$, which were fabricated by standard optical photolithography, Ar ion milling for mesa definition, and electron beam deposition of ohmic Ti/Au contacts. Hall measurements to extract carrier concentrations

^{*}These authors contributed equally to this work.[†]Corresponding author: stemmer@mrl.ucsb.edu

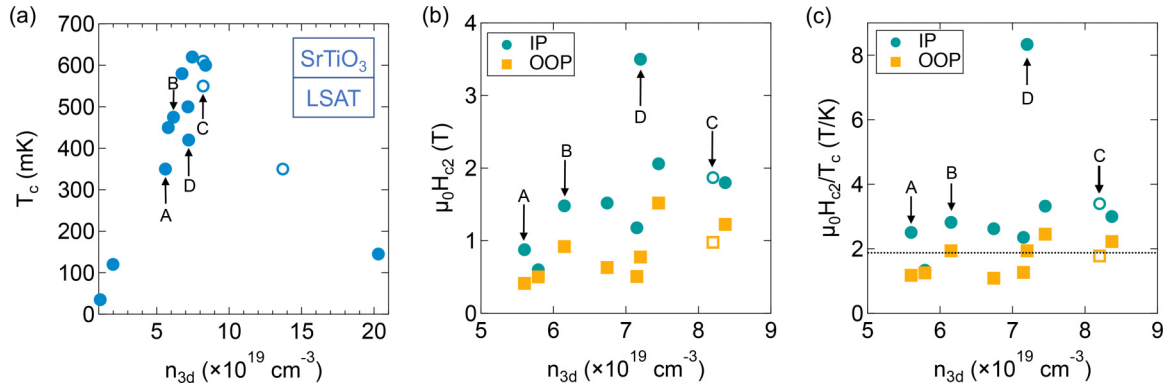


FIG. 1. Superconducting properties as a function of n_{3D} for different field orientations (IP = \mathbf{H} in the film plane; OOP = \mathbf{H} normal to the film plane). (a) T_c , (b) H_{c2} , and (c) the ratio of $\mu_0 H_{c2}$ over T_c . The dotted line in (c) indicates the Pauli limit. Arrows point to data from the four films (A, B, C, D) discussed in more detail. The open symbols are films doped with Sm, and all others are doped with La.

were performed between 300 and 2 K in Quantum Design Dynacool systems. Here, n_{3D} refers to the volume carrier concentration estimated from the Hall measurements at 300 K and the film thickness. Hall bars were aligned along $\langle 100 \rangle$ and $\langle 010 \rangle$, respectively, to facilitate measurements with $\mathbf{I} \parallel \mathbf{H}$ and $\mathbf{I} \perp \mathbf{H}$ with \mathbf{H} in the film plane, where \mathbf{H} is the magnetic field and \mathbf{I} is the excitation current.

Measurements between 1 K and 12 mK were performed in an Oxford Instruments Triton dilution refrigerator using low-frequency lock-in techniques. For measurements of the first harmonic resistances, cryogenic filters were used on the current and voltage lines to reduce the temperature of the electron bath (see Supplemental Material [37]). Superconducting transitions were recorded on different devices and/or contact configurations for all samples to ensure reproducibility.

A nonlinear voltage response to an applied current is a manifestation of nonreciprocal currents in noncentrosymmetric Rashba superconductors [34,38]. The voltage (V) response is given as $V = RI + \gamma RBI^2$ for $\mathbf{I} \perp \mathbf{H}$, where R is the resistance and B is the magnetic flux density [39]. In contrast, $V = 0$ for $\mathbf{I} \parallel \mathbf{H}$ [39]. Here, γ is a coefficient that describes the strength of the magnetochiral anisotropy [39,40]. Given an applied AC current $I = \sqrt{2}I_0 \sin \omega t$, where ω and t are angular frequency and time, respectively, it follows that

$$V = \sqrt{2}RI_0 \sin \omega t - \gamma RBI_0^2 \cos 2\omega t + \gamma RBI_0^2. \quad (1)$$

Nonreciprocal currents were measured by detecting the amplitudes of first and second harmonic resistances with a lock-in amplifier. Following the Eq. (1), the first and second harmonic resistances are defined as $R^\omega = R$ and $R^{2\omega} = \gamma RBI_0 \sqrt{2}$, respectively. The cutoff frequency of the cryogenic filters is on the order of a few tens of Hz, so they were not used for measurements of the second harmonics. For these measurements, lock-in amplifier measurements at a higher frequency were used to enhance the signal-to-noise ratio [37].

We investigated films with a range of carrier densities. Figure 1 shows T_c , H_{c2} , and their ratio as a function of n_{3D} with \mathbf{H} oriented either in or out of the film plane, respectively. Here, T_c is the temperature for which the resistance

reaches 5% of normal-state resistance and H_{c2} is defined as the magnetic field value when the resistance reaches 95% of the normal-state resistance. The sharp drop in T_c at lower concentrations is due to effects from surface depletion [41].

The T_c values [Fig. 1(a)] are in agreement with values previously reported for strained, doped films on LSAT [28]. Enhanced T_c values (up to 600 mK) near the peak of the superconducting dome relative to unstrained, doped SrTiO₃ are directly connected to the ferroelectric normal state, as shown elsewhere [28,29]. The films are polar (point group $4mm$) with the electric polarization vector pointing normal to the film plane [29]. Partially relaxed films, such as films B and D (see Supplemental Material [37]), show a slightly reduced T_c , which is, however, still larger than that of unstrained, doped SrTiO₃. In the following we will focus on slightly underdoped films with n_{3D} tuned between 5.5×10^{19} and $8 \times 10^{19} \text{ cm}^{-3}$.

Figure 1(b) shows H_{c2} as a function of n_{3D} . In general, H_{c2} increases with n_{3D} , as expected for films on the underdoped side of the dome. When \mathbf{H} is in-plane, H_{c2} is strongly enhanced; some samples only enter the normal conducting state at $\mu_0 \mathbf{H} > 2$ T (μ_0 is the vacuum permeability). These H_{c2} values are comparable to the largest values previously reported for doped SrTiO₃ [21]. Figure 1 also shows the values of an unusual sample (film D) with an even more strongly enhanced in-plane H_{c2} . Film D only enters the normal conducting state at $\mu_0 \mathbf{H} > 3.5$ T. The main difference between films B and D is the presence of a thin layer near the interface with the substrate (see Supplemental Material [37]). It is likely that the very large in-plane H_{c2} of film D is associated with the presence of this layer.

The ratio of H_{c2} over T_c is shown in Fig. 1(c). The dotted line marks the Clogston-Chandrasekhar (Pauli) limit, at which the condensation energy of the Cooper pairs $\Delta = 1.78k_B T_c$ equals the magnetic polarization energy of a spin singlet Cooper pair $E = \frac{g\mu_B}{2}H_c$, where μ_B is the Bohr magneton, $g \sim 2$ is the Landé factor, and k_B is Boltzmann's constant [42]. Expressed in units of $\mu_0 H/T$, this ratio is 1.85 T/K. For measurements with \mathbf{H} normal to the film plane, the ratio is below the Pauli limit for most films, while for \mathbf{H} in plane, the ratio is above the limit for several films, and especially so for film D. While the breaking of the Pauli limit and a

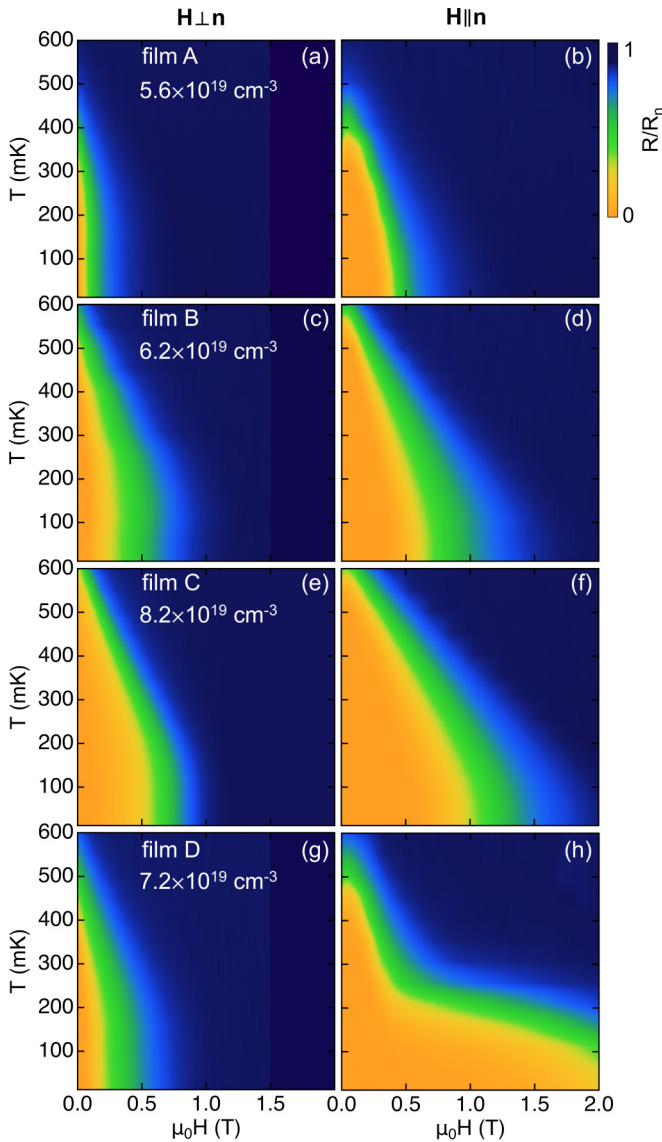


FIG. 2. Normalized (to the normal state) longitudinal resistances R/R_n , represented by the color scale, as a function of temperature (T) and applied magnetic field for films A, B, C, and D. The left columns show the data with \mathbf{H} oriented perpendicular to the film plane, while the right columns are taken with \mathbf{H} oriented in the film plane.

strong anisotropy of H_{c2} is often taken as an indicator of spin triplet superconductivity [8], it should not be taken as the only evidence, especially in materials with strong spin-orbit coupling [9], thin films [21,43,44], and multiband superconductors [11,12].

The transition behavior of the normalized (to the normal-state) resistance R/R_n is shown in Fig. 2 for the four films labeled A, B, C, and D in Fig. 1, measured with \mathbf{H} in and out of plane, respectively. Measurements with \mathbf{H} perpendicular to the film plane (left column) show conventional behavior. In contrast, film D exhibits a “double-dome” structure for \mathbf{H} in plane. This shape drastically differs from the behavior described by the Werthamer-Helfand-Hohenberg (WHH) theory for singlet superconductors. As the large in-plane H_{c2} , the double-dome structure might be associated with distinct order parameters of the bulk and interface layer, respectively.

As an independent measurement supporting an unconventional superconducting state, we measured nonreciprocal transport. Figure 3(a) shows second harmonic resistances of film B. The second harmonic signal is purely imaginary, in agreement with Eq. (1). An antisymmetric component emerges in the second harmonic signal, only if $\mathbf{I} \perp \mathbf{H}$ (see Supplemental Material for a measurement with $\mathbf{I} \parallel \mathbf{H}$ [37]). The extracted γ parameter for this sample is $(1.6 \pm 0.5) \times 10^3 \text{ T}^{-1} \text{ A}^{-1}$. The error was calculated using error propagation and a conservative estimate of the errors in $R^{2\omega}$, R^ω , and in determining the \mathbf{H} position of the peak. Figures 3(b) and 3(c) show the temperature dependence of the second harmonic signal and the extracted γ parameter of sample D. The signal decreases in strength with increasing temperature and vanishes at temperatures above 300 mK. R^ω was recorded in the same measurement setup and used to extract γ parameter [Fig. 3(c)]. Here, γ increases with decreasing temperature and reaches values of $(4.7 \pm 0.5) \times 10^4 \text{ T}^{-1} \text{ A}^{-1}$, which is larger by a factor of 6 than values found in the noncentrosymmetric superconductor MoS_2 [39] and two orders of magnitude higher than that of an interfacial electron gas in SrTiO_3 [38]. The difference in γ parameters between films B and D is mainly due to strongly enhanced H_{c2} of film D. Thus, at the field where $R^{2\omega}$ peaks, which is similar for both films, R^ω of film D is smaller.

In spin-orbit coupled, noncentrosymmetric Rashba superconductors, γ is proportional to the product of the strength of spin-orbit coupling and the ratio between the odd- and even-parity pairing [34]. Unlike films B and D, several other strained (and thus noncentrosymmetric) films, such as film A, showed no detectable nonreciprocal currents (see Supplemental Material [37]). A main result of this study is therefore that the lack of inversion symmetry alone is insufficient to produce a large nonreciprocal current and γ value in polar doped SrTiO_3 films whose normal-state ferroelectric polarization is normal to the film plane [29]. Additional microscopic parameters appear to play a role in determining the nature of the superconductivity. As discussed above, the superconducting properties of film D appear to have contributions from an interface region, resulting in the strongly enhanced in-plane H_{c2} and γ parameter. The nonreciprocal signal is, however, not solely an interface effect because it is also observed in film B, which does not have an interfacial layer. A common feature of both films B and D is partial strain relaxation [37]. Theoretical studies that clarify the role of interfaces, electronic structure, dimensionality, and strain gradients would be an important step in further understanding and tuning the superconducting properties of these films.

To briefly summarize, we find that some doped polar SrTiO_3 films show signatures characteristic of spin-orbit coupled, noncentrosymmetric superconductors. Such a superconductor will exhibit a spin-triplet pairing component and thus has the potential to host non-Abelian Majorana bound states. Further development of existing models of topological superconductivity in SrTiO_3 [8,23,26,27] to describe the polar films studied here would be very desirable. Ultimately, the topological nature of the superconducting phase(s) should be characterized using techniques that can discern the nature of edge states or bound states in the vortex cores.

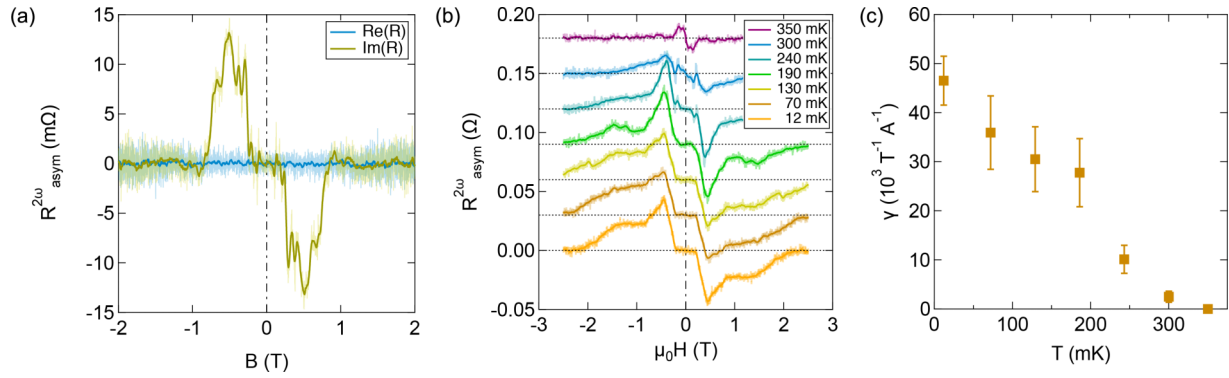


FIG. 3. (a) Asymmetric component of the second-order harmonic $R_{\text{asym}}^{2\omega}$ for film B ($n_{3D} = 6.2 \times 10^{19} \text{ cm}^{-3}$). The magnetic field is in the sample plane and perpendicular to the applied current. The solid lines are obtained by smoothing over 50 data points. The antisymmetric component was obtained via $R_{\text{asym}}^{2\omega}(H) = (1/2)[R^{2\omega}(+|H|) - R^{2\omega}(-|H|)]$. (b) $R_{\text{asym}}^{2\omega}$ for film D as a function of temperature. Traces are offset by 30 mΩ for clarity. (c) Extracted values for the γ parameter [see Eq. (1)] as a function of temperature for film D. Error bars were obtained via error propagation from standard deviations on the values of $R^{2\omega}$ and the position of the peak.

The authors thank Tess Winkelhorst for help with the fabrication of the cryogenic filters. This work was supported by the US Department of Energy (Award No. DE-SC0020305). The

work made use of the MRL Shared Experimental Facilities, which are supported by the MRSEC Program of the US National Science Foundation under Award No. DMR 1720256.

- [1] A. Y. Kitaev, *Ann. Phys.* **303**, 2 (2003).
- [2] L. Fu and C. L. Kane, *Phys. Rev. Lett.* **100**, 096407 (2008).
- [3] X.-L. Qi and S.-C. Zhang, *Rev. Mod. Phys.* **83**, 1057 (2011).
- [4] J. Alicea, *Rep. Prog. Phys.* **75**, 076501 (2012).
- [5] M. Sato and Y. Ando, *Rep. Prog. Phys.* **80**, 076501 (2017).
- [6] V. M. Edel'shtein, *Zh. Eksp. Teor. Fiz.* **95**, 2151 (1989)[*Sov. Phys. - JETP* **68**, 1244 (1989)].
- [7] L. P. Gor'kov and E. I. Rashba, *Phys. Rev. Lett.* **87**, 037004 (2001).
- [8] V. Kozii and L. Fu, *Phys. Rev. Lett.* **115**, 207002 (2015).
- [9] M. Smidman, M. B. Salamon, H. Q. Yuan, and D. F. Agterberg, *Rep. Prog. Phys.* **80**, 036501 (2017).
- [10] G. Binnig, A. Baratoff, H. E. Hoening, and J. G. Bednorz, *Phys. Rev. Lett.* **45**, 1352 (1980).
- [11] Y. Ayino, J. Yue, T. Wang, B. Jalan, and V. S. Pribiag, [arXiv:1812.02875](https://arxiv.org/abs/1812.02875).
- [12] J. M. Edge and A. V. Balatsky, *J. Supercond. Novel Magn.* **28**, 2373 (2015).
- [13] J. F. Schooley, W. R. Hosler, E. Ambler, J. H. Becker, M. L. Cohen, and C. S. Koonce, *Phys. Rev. Lett.* **14**, 305 (1965).
- [14] H. Uwe, T. Sakudo, and H. Yamaguchi, *Jpn. J. Appl. Phys. Suppl.* **24**, 519 (1985).
- [15] H. Uwe, R. Yoshizaki, T. Sakudo, A. Izumi, and T. Uzumaki, *Jpn. J. Appl. Phys. Suppl.* **24**, 335 (1985).
- [16] S. J. Allen, B. Jalan, S. B. Lee, D. G. Ouellette, G. Khalsa, J. Jaroszynski, S. Stemmer, and A. H. MacDonald, *Phys. Rev. B* **88**, 045114 (2013).
- [17] X. Lin, G. Bridoux, A. Gourgout, G. Seyfarth, S. Kramer, M. Nardone, B. Fauque, and K. Behnia, *Phys. Rev. Lett.* **112**, 207002 (2014).
- [18] A. D. Caviglia, M. Gabay, S. Gariglio, N. Reyren, C. Cancellieri, and J. M. Triscone, *Phys. Rev. Lett.* **104**, 126803 (2010).
- [19] A. Joshua, S. Pecker, J. Ruhman, E. Altman, and S. Ilani, *Nat. Commun.* **3**, 1129 (2012).
- [20] G. Khalsa, B. Lee, and A. H. MacDonald, *Phys. Rev. B* **88**, 041302(R) (2013).
- [21] M. Kim, Y. Kozuka, C. Bell, Y. Hikita, and H. Y. Hwang, *Phys. Rev. B* **86**, 085121 (2012).
- [22] C. Yin, P. Seiler, L. M. K. Tang, I. Leermakers, N. Lebedev, U. Zeitler, and J. Aarts, [arXiv:1904.03731](https://arxiv.org/abs/1904.03731).
- [23] M. S. Scheurer and J. Schmalian, *Nat. Commun.* **6**, 6005 (2015).
- [24] K. A. Muller and H. Burkard, *Phys. Rev. B* **19**, 3593 (1979).
- [25] C. H. Ahn, A. Bhattacharya, M. Di Ventura, J. N. Eckstein, C. D. Frisbie, M. E. Gershenson, A. M. Goldman, I. H. Inoue, J. Mannhart, A. J. Millis, A. F. Morpurgo, D. Natelson, and J. M. Triscone, *Rev. Mod. Phys.* **78**, 1185 (2006).
- [26] S. Kanasugi and Y. Yanase, *Phys. Rev. B* **98**, 024521 (2018).
- [27] S. Kanasugi and Y. Yanase, *Phys. Rev. B* **100**, 094504 (2019).
- [28] K. Ahadi, L. Galletti, Y. Li, S. Salmani-Rezaie, W. Wu, and S. Stemmer, *Sci. Adv.* **5**, eaaw0120 (2019).
- [29] R. Russell, N. Ratcliff, K. Ahadi, L. Y. Dong, S. Stemmer, and J. W. Harter, *Phys. Rev. Mater.* **3**, 091401 (2019).
- [30] C. W. Rischau, X. Lin, C. P. Grams, D. Finck, S. Harms, J. Engelmayer, T. Lorenz, Y. Gallais, B. Fauque, J. Hemberger, and K. Behnia, *Nat. Phys.* **13**, 643 (2017).
- [31] Y. Tomioka, N. Shirakawa, K. Shibuya, and I. H. Inoue, *Nat. Commun.* **10**, 738 (2019).
- [32] A. Stucky, G. W. Scheerer, Z. Ren, D. Jaccard, J. M. Pouchard, C. Barreateau, E. Giannini, and D. van der Marel, *Sci. Rep.* **6**, 37582 (2016).
- [33] S. Hoshino, R. Wakatsuki, K. Hamamoto, and N. Nagaosa, *Phys. Rev. B* **98**, 054510 (2018).
- [34] R. Wakatsuki and N. Nagaosa, *Phys. Rev. Lett.* **121**, 026601 (2018).
- [35] B. Jalan, R. Engel-Herbert, N. J. Wright, and S. Stemmer, *J. Vac. Sci. Technol. A* **27**, 461 (2009).
- [36] J. Son, P. Moetakef, B. Jalan, O. Bierwagen, N. J. Wright, R. Engel-Herbert, and S. Stemmer, *Nat. Mater.* **9**, 482 (2010).

- [37] See Supplemental Material at <http://link.aps.org/supplemental/10.1103/PhysRevB.101.100503> for the films' microstructure, details about the cryofilters, estimates of the electron temperature, heating effects in field sweeps, orbital fields, and additional data on the nonreciprocal transport measurements.
- [38] D. Choe, M.-J. Jin, S.-I. Kim, H.-J. Choi, J. Jo, I. Oh, J. Park, H. Jin, H. C. Koo, B.-C. Min, S. Hong, H.-W. Lee, S.-H. Baek, and J.-W. Yoo, *Nat. Commun.* **10**, 4510 (2019).
- [39] R. Wakatsuki, Y. Saito, S. Hoshino, Y. M. Itahashi, T. Ideue, M. Ezawa, Y. Iwasa, and N. Nagaosa, *Sci. Adv.* **3**, e1602390 (2017).
- [40] G. Rikken and E. Raupach, *Nature (London)* **390**, 493 (1997).
- [41] A. Ohtomo and H. Y. Hwang, *Appl. Phys. Lett.* **84**, 1716 (2004).
- [42] A. M. Clogston, *Phys. Rev. Lett.* **9**, 266 (1962).
- [43] A. M. Toxen, *Phys. Rev.* **127**, 382 (1962).
- [44] G. Rickayzen, *Phys. Rev.* **138**, A73 (1965).

Supplementary Information

Possible signatures of mixed-parity superconductivity in doped, polar SrTiO₃ films

Timo Schumann, Luca Galletti, Hanbyeol Jeong, Kaveh Ahadi, William M. Strickland, Salva Salmani-Rezaie, and Susanne Stemmer

Materials Department, University of California, Santa Barbara, California 93106-5050, USA

X-ray diffraction

Figure S1 shows 2θ - ω scans of the 002 reflections of films B, D, and a reference film E. Film E did not show any nonreciprocal signal (see below). The expected peak positions for fully strained SrTiO₃ films on LSAT and those of fully relaxed SrTiO₃ are indicated by the dotted lines. Film E is fully strained, while the peak positions of films B and D indicate partial strain relaxation.

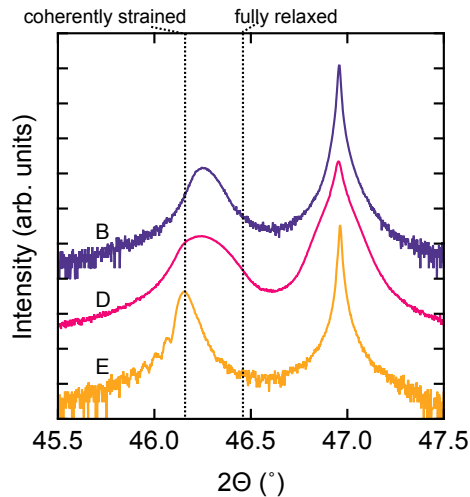


Figure S1 (a): X-ray diffraction patterns around the 002 reflection of SrTiO₃ and LSAT, respectively. The dotted lines indicate the expected peak positions for coherently strained and fully relaxed SrTiO₃, respectively.

Transmission Electron Microscopy

Figure S2 shows cross-section high-angle annular dark-field (HAADF) images of SrTiO₃/LSAT interfaces acquired in scanning transmission electron microscopy (STEM). Figures S2a,b show film D, which shows a slightly disordered interface layer of ~ 5 nm thickness that is a result of three-dimensional nucleation at the beginning of growth. Figure S2c shows a more typical SrTiO₃/LSAT interface that is atomically abrupt.

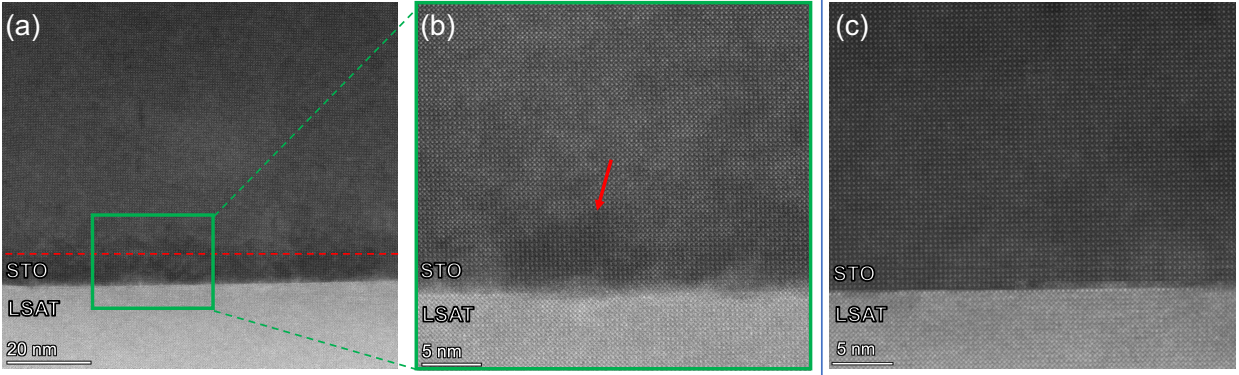


Figure S2: HAADF-STEM images of SrTiO₃ films grown on LSAT. (a) HAADF-STEM image of film D. A magnified section (indicated by the green rectangle in (a)) is shown in (b). (c) HAADF-STEM image of a typical strained SrTiO₃ film on LSAT that has an abrupt interface.

Cryogenic filters and estimation of the electron temperature

Cryogenic filters were installed at the mixing chamber stage on existing phosphorus bronze twisted pair DC lines to reduce the electron temperature and high frequency noise. The cryo-filters consisted of low-pass RC filters with a nominal cutoff frequency of 1 kHz, in series with commercial ceramic RLC mini-circuit components (LFCN-225D+, LFCN-1800D) with cutoff frequencies of 225 MHz and 1800 MHz, respectively. Two additional stages of filtering were achieved using a twisted pairs ribbon filter [1] and a microstrip meander filter [2], respectively, both with expected cutoff frequency in the GHz range, aimed at reducing the effective electron temperature at the sample stage [1]. The cryo-filters effectively reduce the available frequency bandwidth to below a few tens of Hz (or even less in the case of non-reciprocal measurements, since the detection is performed on the second harmonic of the signal).

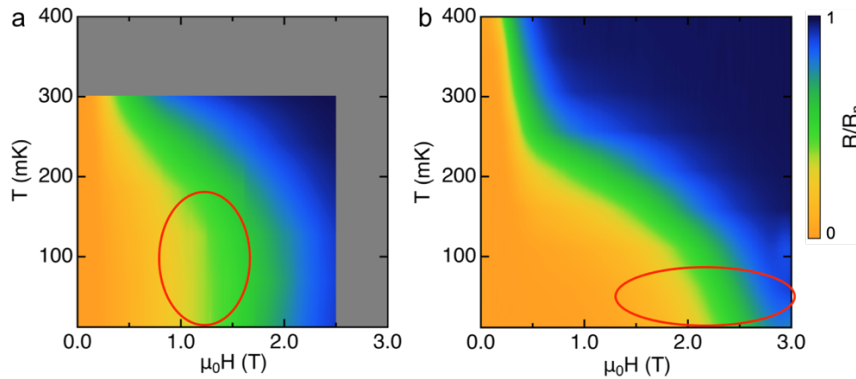


Figure S3: Normalized map of the resistance as a function of magnetic field and temperature for film D without (a) and with (b) cryo-filters.

Figure S3 shows a map of the normalized resistance as a function of magnetic field and temperature for sample D measured without and with the cryo-filters. The flattening of the superconducting dome below 150 mK (in the red circle in Fig. S3a) indicates that the effective electron temperature without the cryo-filters is higher.

Measurement of H_{c2} was performed by sweeping the magnetic field at a constant rate. In this configuration, precautions must be taken to avoid artifacts due to heating. One source of heating is eddy currents induced

in the sample and in the sample holder during the field ramp. This can be addressed by choosing an appropriately slow ramp. To exclude heating due to the magnet sweep, we measured $R(T)$ at a constant field, as shown in Fig. S4, which are compatible with the values in the resistance map (Fig. S3a). The curves saturate below 50 mK which we attribute to residual saturation of the electron temperature with cryo-filters. This is also responsible for the apparent rounding of the double dome below 50 mK (see red circle in Fig. S3b).

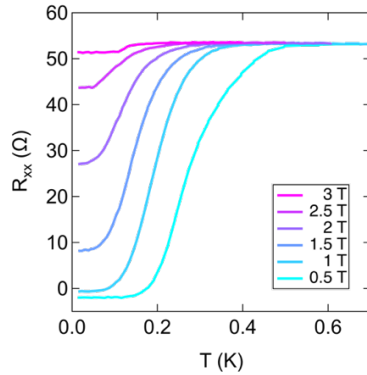


Figure S4: $R(T)$ curves for sample D at a constant field.

Frequency dependence

Second harmonic resistances recorded at different excitation frequencies are shown in Fig. S5. Despite some additional noise at lower frequency, presumably from the $1/f$ background noise, the $R^{2\omega}$ signal is frequency independent.

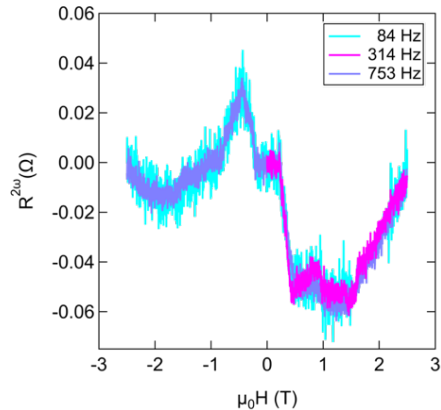


Figure S5: Second order harmonic resistance measured at different excitation frequencies (sample D).

Calculation of the orbital field

The orbital field was defined via the relation $H_{orb} = -0.7 T_C \frac{dH_C}{dT} \Big|_{T=T_C}$. For all samples, H_{orb} was found to be comparable with the measured H_{c2} except for the in-plane measurement of sample D. In this case, H_{c2} exceeds H_{orb} by a factor of five, as shown in Fig. S6. Therefore, the increased H_{c2} of sample D cannot be explained by a conventional WHH model.

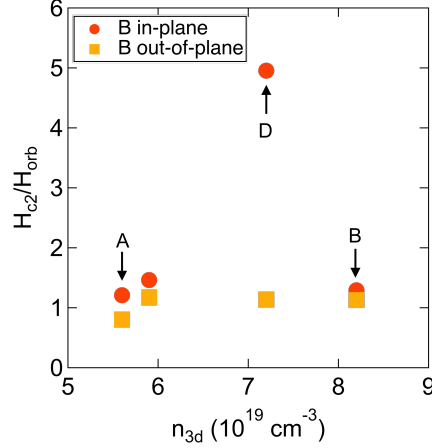


Figure S6: Ratios of measured upper critical field and orbital field for different films discussed in the main text.

Sample without a second harmonic signal

We performed non-reciprocal transport measurements on six different samples. Among those, two samples, which also show partial strain relaxation, showed pronounced non-reciprocal transport, as shown in the main text. In Fig. S7, we compare the antisymmetric components of the second harmonic of samples D and E. Sample E is fully strained (see Fig. S1), has a carrier density of $5 \times 10^{19} \text{ cm}^{-3}$ (measured at 1 K), a T_c of 600 mK and is therefore also ferroelectric. No signal above the noise level is detectable.

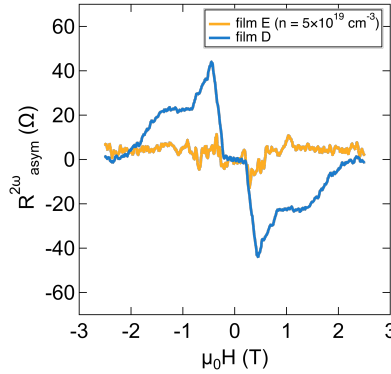


Figure S7: Antisymmetric part of the second harmonic resistance of films D and E.

Additional data from second harmonic measurements

We performed additional measurements to further evaluate the second harmonic measurements and their consistency with Eq. (1) (non-centrosymmetric superconductivity):

1. Measurements of the real and imaginary components of $R^{2\omega}$
2. Measurements of $R^{2\omega}$ in Hall configuration to exclude that the antisymmetric component is due to a Hall signal
3. Measurements of $R^{2\omega}$ for $\mathbf{H} \parallel \mathbf{I}$
4. Measurements of the dependence of $R^{2\omega}$ as a function of the excitation current

The results from these measurements are shown next.

Real and imaginary components of the second harmonic resistance

Real and imaginary components of the raw data from sample D are shown in Fig. S8. The signal is purely imaginary, in accordance with Eq. (1).

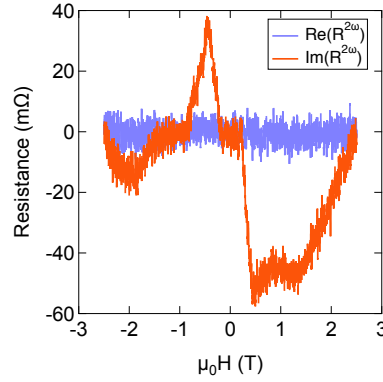


Figure S8: Real and imaginary components of the second order harmonic resistance (sample D).

Measurement of the second harmonic Hall resistance

These measurements showed no signal above the noise floor (see Fig. S9) below 1 T. Therefore, we can exclude that the asymmetric signal shown in Fig. 3 of the main text originates from mixing of a Hall voltage.

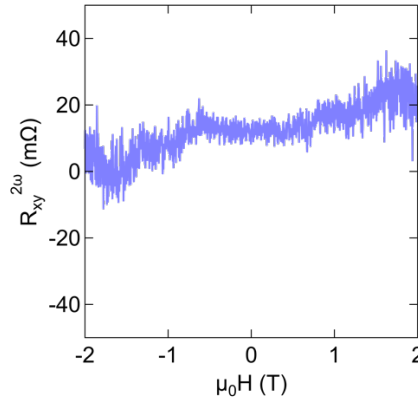


Figure S9: Second harmonic resistance of sample D recorded in Hall geometry.

Measurement with magnetic field parallel to the current

Second harmonic resistances of sample D were measured with \mathbf{H} in the film plane and $\mathbf{I} \parallel \mathbf{H}$ and are shown in Fig. S10. The axes are scaled for direct comparison with the amplitude observed for $\mathbf{I} \perp \mathbf{H}$, shown in the main text. No appreciable asymmetric component is present.

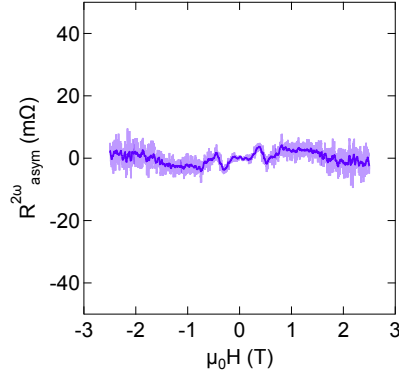


Figure S10: Antisymmetric component of the second order harmonic resistance measured $I \parallel H$ (sample D). The lighter line shows the raw data, while the darker line shows smoothed data.

Measurement with different excitation currents

Measurements with excitation currents I_0 of $0.5 \mu\text{A}$ and $1.0 \mu\text{A}$ are shown in Fig. S11. The second harmonic resistance is about 30 % larger for $I_0 = 1 \mu\text{A}$, which is lower than the expected increase of a factor of two. The origin of this quantitative discrepancy is unclear.

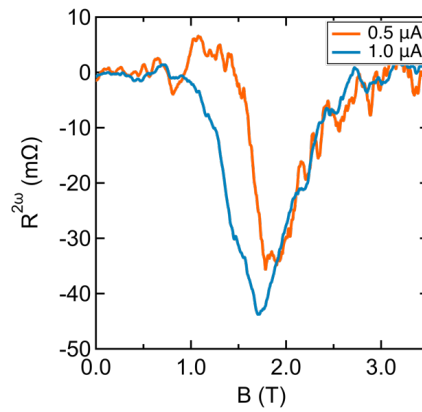


Figure S11: Second harmonic resistance of sample D for different excitation currents. The data was smoothed by a moving average procedure.

References

- [1] L. Spietz, J. Teufel, and R. J. Schoelkopf, arXiv:cond-mat/0601316 (2006).
- [2] H. A. Wheeler, IEEE Trans. Microwave Theory Techniques **25**, 631 (1977).